Research Article

Thickness Dependent Interlayer Magnetoresistance in Multilayer Graphene Stacks

S. C. Bodepudi,[1] X. Wang,[2] A. P. Singh,[1] and S. Pramanik[1]

[1]*Department of Electrical and Computer Engineering, University of Alberta, Edmonton, AB, Canada T6G 2V4*
[2]*School of Microelectronics and Solid State Electronics, UESTC, Chengdu, Sichuan 610054, China*

Correspondence should be addressed to S. Pramanik; spramani@ualberta.ca

Chemical Vapor Deposition grown multilayer graphene (MLG) exhibits large out-of-plane magnetoresistance due to interlayer magnetoresistance (ILMR) effect. It is essential to identify the factors that influence this effect in order to explore its potential in magnetic sensing and data storage applications. It has been demonstrated before that the ILMR effect is sensitive to the interlayer coupling and the orientation of the magnetic field with respect to the out-of-plane (c-axis) direction. In this work, we investigate the role of MLG thickness on ILMR effect. Our results show that the magnitude of ILMR effect increases with the number of graphene layers in the MLG stack. Surprisingly, thicker devices exhibit field induced resistance switching by a factor of at least $\sim 10^7$. This effect persists even at room temperature and to our knowledge such large magnetoresistance values have not been reported before in the literature at comparable fields and temperatures. In addition, an oscillatory MR effect is observed at higher field values. A physical explanation of this effect is presented, which is consistent with our experimental scenario.

Graphene, a single atomic layer of hexagonally arranged carbon atoms, is one of the most investigated material systems in recent years. Charge carriers in graphene behave like two-dimensional (2D) Dirac fermions and exhibit various novel phenomena that are generally not observed in conventional materials [1–4]. It is interesting to note that many of the effects that are observed in monolayer graphene have also been reported in multilayer graphene (MLG) [5–9]. For some of the applications, multilayer graphene can be a better alternative due to its robustness and simpler fabrication steps [8–11]. In recent years, much attention has been given to multilayer graphene structures for next generation sensor and data storage applications [8, 12–19]. In particular, various magnetoresistance (MR) effects have been extensively explored in multilayer graphene due to their potential to exist even at room temperature [14, 18–20]. However, many of these effects are significant at very large magnetic fields (~100 kG) that are outside the range generally required for practical applications [21, 22]. We recently demonstrated a large negative MR in multilayer graphene at low-field range (~2 kG) [16, 17], which often persists even at room

temperature. The origin of this large negative MR is related to the existence of 2D Dirac fermions in multilayer graphene.

In general, the linear energy dispersion of monolayer graphene no longer exists in MLG (or, graphite) due to strong interlayer coupling between neighboring graphene layers [4, 23, 24]. However, in case of "turbostratic" MLG, in which graphene layers are randomly oriented, interlayer coupling is weakened and the massless Dirac fermion nature of each graphene layer is preserved [25, 26]. Such turbostratic MLG can be realized by chemical vapor deposition (CVD) process using polycrystalline Ni as a catalyst [27, 28]. We demonstrated previously [16, 17] that such a weakly coupled MLG stack exhibits a unique quantum mechanical MR effect, known as interlayer magnetoresistance (ILMR). To further understand and explore potential applications based on ILMR effect, it is important to identify the factors that influence this effect. In our present study we report effect of MLG thickness on ILMR. Thickness of the MLG stack can be varied by the CVD growth parameters. To our knowledge, such thickness dependent ILMR studies have never been performed in any multilayer Dirac carrier system.

In the past, ILMR effect has been studied extensively in α-(BEDT-TTF)$_2$I$_3$, which is an organic material that behaves like 2D Dirac carrier system under certain conditions [29, 30]. However, this effect is not very well explored in other 2D Dirac carrier systems, such as graphene. We recently reported first observation of ILMR effect in multilayer graphene (MLG) stacks with weak interlayer coupling, which represents a stack of 2D Dirac electron systems [16, 17]. Since the Fermi level in each graphene layer is located in the vicinity of the Dirac point, the out-of-plane charge transport in this system occurs via interlayer tunneling between the states near the Dirac points of each graphene layer. Since the density of states (DOS) in the vicinity of Dirac point is very low [4], the net interlayer tunneling current of the MLG stack is also small. When an out-of-plane magnetic field is applied, the linear energy dispersion of each graphene layer transforms into a series of Landau levels [4]. If a Landau level coincides with the (quasi) Fermi energy, interlayer tunneling occurs through the Landau levels of the consecutive graphene layers. Since the degeneracy of the Landau levels increases with the strength of the out-of-plane magnetic field, a considerable increase in interlayer tunneling current is observed at higher fields due to the increase in available number of carriers for interlayer tunneling [31]. This effect results in a large drop in out-of-plane resistance (R_{zz}) and is termed as interlayer magnetoresistance (ILMR). Reference [31] modeled this effect for the special case ("quantum limit") in which interlayer transport occurs via the "zero-mode" Landau levels of each layer. Zero-mode Landau level appears at the Dirac point and its position is independent of the magnetic field strength. It has been shown in [32] that ILMR persists even when interlayer tunneling takes place between higher order Landau levels ($n \rightarrow n$ tunneling, $n \neq 0$; n being Landau level index). Tunneling between different Landau levels ($n \rightarrow n'$, $n \neq n'$; $n, n' \neq 0$), combined with in-plane charge motion, results in a positive MR at small field range [32].

To explore the effect of MLG thickness on the ILMR effect, three batches (S1, S2, and S3) of samples have been studied in this work, each batch having a specified nominal thickness, different from the other batches. To grow MLG, we used low pressure chemical vapor deposition (LPCVD) process on catalytic Ni substrate of thickness ~25 μm. To grow MLG with different thicknesses, we systematically varied the concentration of carbon containing species (methane, in our case) from 0.1% to 0.3% in the CVD process by keeping all other parameters unchanged. This affects the amount of dissolved and precipitated carbon during the CVD process, and results in MLGs with different nominal thicknesses. A detailed description of the CVD process has been presented in our previous work [16, 33]. The structural quality and uniformity of as-grown MLG samples have been investigated by Raman spectroscopy (with laser excitation wavelength of 532 nm) and in-built optical microscopy. The estimated penetration depth of Raman laser within graphite is ~50 nm from the top surface [34], and hence Raman data reveals the quality of the graphene layers within this thickness range from the top surface. Raman spectra of various as-grown MLG samples (on Ni) are displayed in Figures 1(a), 1(b), and 1(c). These samples exhibit strong G peak at 1580 cm^{-1} and

a symmetric 2D band around 2700 cm^{-1} (Figures 1(a), 1(b), and 1(c)). The strong G peak implies formation of hexagonal graphene lattice in all cases. The symmetric 2D band has been observed in all cases (Figures 1(a), 1(b), and 1(c) and *top insets* of these figures), which confirms weak interlayer coupling over an extended volume of the samples [16, 17, 26]. The absence of defect (D) peak at 1350 cm^{-1} in all of our as-grown MLG samples (Figures 1(a), 1(b), and 1(c) and *bottom insets* of these figures) indicates high structural quality and negligible defect density [26], at least within ~50 nm (penetration depth of the Raman laser) from the top surface. These features are common for all three batches of MLG samples considered in this study. Similar features have been observed in spectra obtained from other regions. In Figure 1(d), typical Raman spectrum of MLG/Ni *interfacial layers* of a transferred MLG sample is shown. Strong defect (D) peak is observed from these interfacial layers and this feature is again common for all three batches used in this study. The defect peak originates due to two reasons: (1) it is well known [35] that, at the Ni/MLG interface, the 3d states of Ni hybridize strongly with the 2p_z states of carbon atoms, which results in disappearance of the Dirac cone dispersion of the interfacial graphene layer(s), opening of a band gap and creation of defect states in the band gap, and (2) Ni surface has grain boundaries with atomic scale discontinuities, which result in small area graphene growth near the interface and creation of edge states [36, 37]. However, these defects are nonexistent as one moves away from the Ni/MLG interface. For example, hybridization effect only affects the interfacial layers and the layers away from the interface are not affected by this effect due to rapidly vanishing overlap between the atomic orbitals [16, 17, 35]. Similarly, top layers tend to grow continuously over the (small area) bottom layers, without creation of any edge states [36, 37]. As a result, the top layers do not exhibit any D band in the Raman spectra (Figures 1(a), 1(b), and 1(c), and *bottom insets*).

To estimate the nominal thicknesses of these as-grown MLG samples, we performed step height measurements after transferring the MLG stack on SiO$_2$/Si substrate. A detailed description of the transfer process has been presented in [16]. Optical images of the transferred samples are displayed in Figures 2(a), 2(b), and 2(c). The typical thickness distributions of the transferred MLG samples are shown in the insets of these figures. From these distributions, the average thicknesses of the three batches are estimated to be (i) ~60 nm (batch S1), (ii) ~200 nm (batch S2), and (iii) ~ 300 nm (batch S3). The multigrain feature observed in these images originates from the bottom MLG surface (i.e., the surface that was in contact with Ni before transfer). Raman studies on the transferred specimens have not detected any Raman D peak [16] which implies that these defects (grain boundaries) are not present within ~50 nm (penetration depth of Raman laser) depth from the top surface. However, as shown in Figure 1(d), Raman spectrum taken from a transferred and "flipped" sample (i.e., in which the bottom interfacial layer faces up) shows strong defect peak. Thus, we believe that, in our as-grown MLG sample, the top layers are homogeneous, defect-free and formation of Landau levels is possible, whereas the interfacial layer is defective.
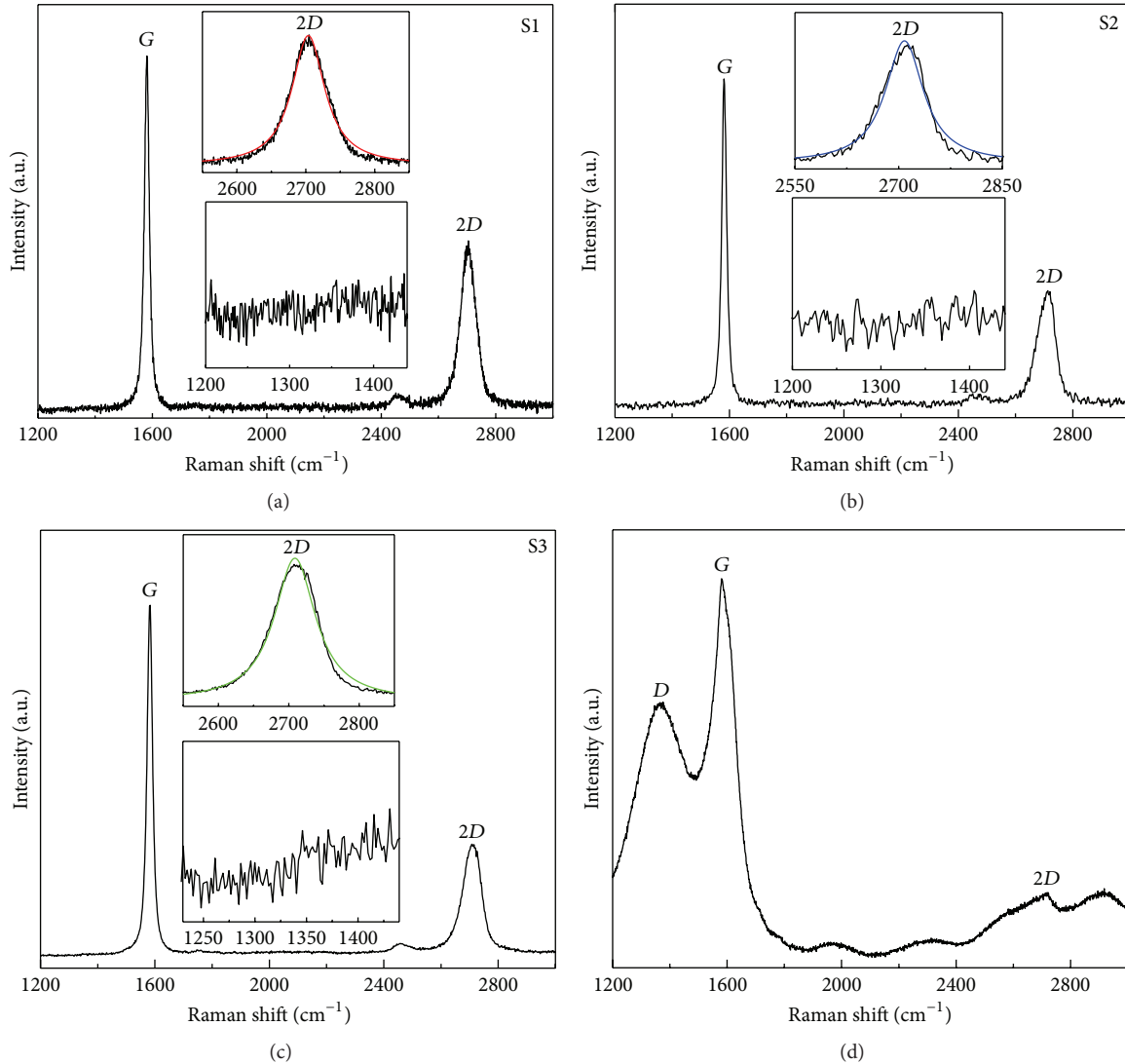
Figure 1: Typical Raman spectra of as-grown MLG (taken from the top surface, i.e., from the "defect-free region") with nominal thicknesses of (a) ~60 nm (batch S1), (b) ~200 nm (batch S2), and (c) ~300 nm (batch S3). (d) Typical Raman spectrum taken from the layers at the MLG/Ni interface ("defective region"). As seen from Figures (a)–(c), defect (D) peak at 1350 cm^{-1} is absent in all these cases. The *bottom insets* in these figures show a 10x magnified view of the spectrum close to 1350 cm^{-1} range, and still no defect peak can be discerned above the noise level. The Raman 2D band of each batch is symmetric and can be fitted with a single Lorentzian as shown in the *top insets* of Figures (a), (b), and (c). These Raman features are valid for almost all areas of the samples. In Figure (d) strong D peak is observed from the transferred MLG sample, taken from the bottom surface (after removing the Ni and flipping over the MLG stack). This confirms the defective nature of the interfacial layers.

Based on the above experimental evidence we conclude that as-grown MLG on Ni consists of two distinct regions: "defective" interfacial region that shows Raman D peak (Figure 1(d)) and grain boundaries (Figures 2(a)–2(c)) and a "defect-free" region that does not show any Raman D peak (Figures 1(a)–1(c)). The layers in the defect-free region are weakly coupled as evidenced by the distortion-free 2D Raman band as seen in Figures 1(a)–1(c), *top insets*. The defective interfacial region shows metallic temperature dependence ($dR_{zz}/dT > 0$) due to the presence of Ni atoms and/or conductive "edge states" at the missing atom sites, as shown in our previous work [16]. The overall CPP resistance, on the

other hand, exhibits insulator-like temperature dependence ($dR_{zz}/dT < 0$, shown later) and is much larger compared to the CPP resistance of the interfacial region [16]. We therefore conclude that the overall CPP resistance is dominated by the "defect-free" region and not by the defective interfacial region. We observed that the charge transport characteristics of as-grown MLG samples with thickness <30 nm were dominated by the defective interfacial region [16]. Therefore, in this study we only considered samples with as-grown MLG thicker than 50 nm to ensure that the CPP resistance is dominated by the defect-free region. It is important to note that the transferred samples generally show distorted 2D Raman band
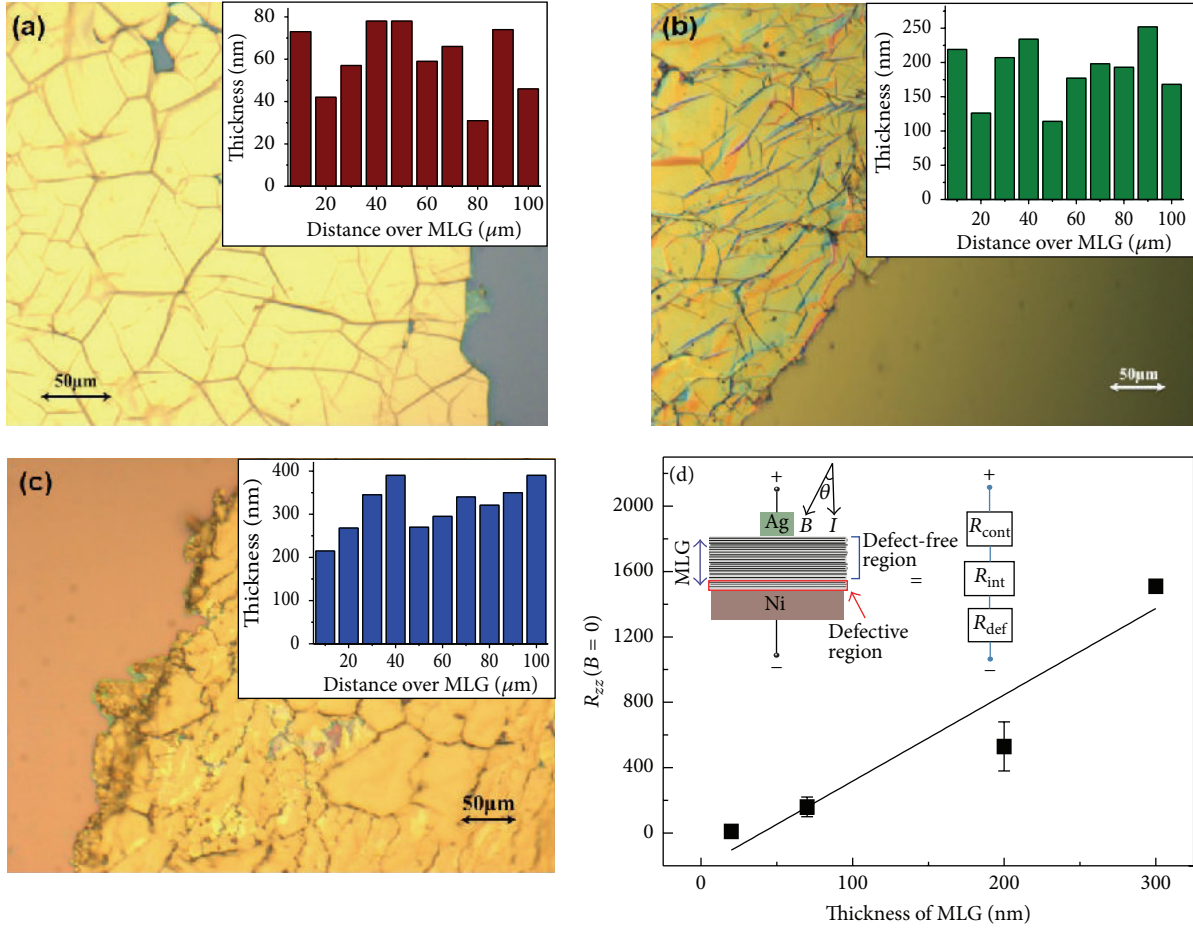
FIGURE 2: Optical images of transferred MLG and thickness dependent *zero-field* CPP resistance $R_{zz}(B = 0)$. Optical images of the three transferred MLG samples are presented in Figures (a) ~60 nm (batch S1), (b) ~200 nm (batch S2), and (c) ~300 nm (batch S3). *Insets* of these figures show typical thickness variations in these samples. Figure (d) shows *zero-field* resistance $R_{zz}(B = 0)$ as a function of MLG thickness. For ~300 nm devices, minimum value of $R_{zz}(0)$ is ~1.6 kΩ and often it is much larger than this value due to the reasons discussed in the paper. $R_{zz}(0)$ has been found to increase with increasing MLG thickness. This indicates that the overall resistance of the device is dominated by the "bulk" and not by the interfaces and the contacts. The inset shows device schematic and an equivalent circuit model of the device. As discussed in the main text, the combination of contact resistance and defective region resistance ($R_{cont} + R_{def}$) of all three sets of samples is <10 Ω and shows metallic temperature dependence. The overall device, however, shows insulating temperature dependence. This proves that $R_{cont} + R_{def}$ does not play a dominant role in the overall CPP measurements. In Figure (d), for 25 nm data point, error bar is smaller than the marker size. For 300 nm data point, error bar is not shown due to the large variability in $R_{zz}(0)$ as discussed in the paper.

[16, 17, 38], which is a signature of strong interlayer coupling and hence ILMR has not been observed in the transferred samples. The role of the Ni substrate is that it allows growth of weakly coupled multilayered graphene stack and hence such systems permit investigation of the ILMR effect. Thus, our ILMR experiments have been performed with Ni as the bottom contact. As mentioned above, we have performed several control experiments to ensure that the observed CPP MR does not originate from Ni or the Ni/MLG interfacial layers.

The device schematic is shown in Figure 2(d) *top inset*. The catalytic Ni substrate and silver epoxy have been used as bottom and top contacts, respectively. The top contact area is ~1 mm² and is carefully placed at the center of the top MLG surface to maintain uniform current distribution during CPP measurements. A constant DC current bias of 1 mA has been used in all MR measurements. The total CPP resistance of the

device is a series combination of the contact resistance (R_{cont}), resistance from the defective interfacial region (R_{def}), and the "bulk" interlayer resistance (R_{int}) as shown in Figure 2(d) *top inset*. Both R_{cont} and R_{def} exhibit metallic temperature dependence as mentioned above and are almost identical for the three batches considered in this study. It has been independently verified that R_{cont} and R_{def} vary in between 2–4 Ω and 6-7 Ω, respectively (at zero field) [16, 17]. However, the overall (zero field) CPP resistance of our MLG samples exhibits insulator-like temperature dependence and it is at least two orders of magnitude larger (see later) than R_{cont} and R_{def}. Therefore, the overall CPP resistance is dominated by the interlayer resistance (R_{int}) component originating from the "defect-free" bulk region (away from the interface). To further verify this, we compared the zero-field CPP resistance of MLG samples (same contact area) with different

thicknesses (Figure 2(d), *main image*). The CPP resistance has been found to increase with MLG thickness. This indicates that CPP resistance R_{zz} is dominated by the "bulk" region of the sample and not by the interfaces or the contacts.

Formation of nanocontacts between the top and bottom electrodes is highly unlikely since our MLG stack is quite thick (60–300 nm range) and in all cases we have obtained complete surface coverage (without any discontinuity) by MLG. This has been confirmed by Raman data. In case of discontinuities (or "holes") in the MLG, we typically observe a defect peak in the Raman signal due to the edge states. But no such signature has been found. For the bulk Ni foil, magnetization switching occurs at coercive field of ~ few G (see, e.g., [39, 40]) and this cannot be related to the observed MR curves (described below), in which resistance change occurs at much higher field range (~few kG). Also, in-plane MR response shows a positive MR (Figure SI-3 in Supplementary Material available online at http://dx.doi.org/10.1155/2016/8163742), implying that in-plane component of carrier transport is not dominant.

Figure 3(a) shows typical CPP MR of a thinner (~60 nm) MLG stack in the temperature range 50–200 K. The zero-field resistance of this sample is ~200 Ω at 50 K which gradually decreases to 100 Ω at 200 K. The sample clearly shows strong insulator-like temperature dependence ($dR_{zz}/dT < 0$) at zero field. CPP MR is ~40% at 50 K (over the entire field range of 10 kG) and magnitude of the negative MR drops gradually with increase in temperature. In this study negative MR has been computed as $[\Delta R_{zz}/R_{zz}(0) = |R_{zz}(B) - R_{zz}(0)|/R_{zz}(0)] \times 100\%$, which can have a theoretical maximum of 100%. MR effect is barely perceptible at 200 K and vanishes above this temperature and hence data above this temperature are not shown. Switching field (B_{sw}), the field value at which the CPP resistance sharply drops, increases gradually with increase in temperature. For this study, B_{sw} is taken to be the full-width-half-maximum (FWHM) of the negative MR curves [16]. With increasing temperature, negative MR broadens and hence B_{sw} increases. At higher temperatures, the low-field positive MR dominates over the negative MR due to enhanced Landau level mixing, which is responsible for the increase in B_{sw} and hence broadening of the MR curves [32]. The inset in Figure 3(a) shows R_{zz}^{-1} versus B in the field range in which negative MR is most prominent. A clear linear fit has been observed, as expected from theory [31]. Further, slope of R_{zz}^{-1} versus B tends to decrease with increasing temperature, which is also consistent with theory. Thus, the observed MR effect is consistent with ILMR phenomenon.

Interestingly, in the low-temperature (50 K) scan in Figure 3(a), an oscillatory MR component has been observed for field values ~4 kG and larger. Such oscillations are reminiscent of Shubnikov-de Haas (SdH) oscillations that are often observed in graphitic systems [41–43]. In our case of CPP charge transport, such oscillations imply that the Fermi level is not located at the Dirac point (or at the zero-mode Landau level), as a result of unintentional doping of the graphene layers during the fabrication process. In this case, CPP resistance will exhibit a valley at field values for which a Landau level coincides with the Fermi level, since under this condition plenty of states will be available for

interlayer tunneling. However, at other field values Landau levels will not coincide with the Fermi level, which will result in a peak in the MR oscillations due to lack of available states for tunneling. In the low-field range ($B < B_{sw}$, i.e., before resistance switching due to negative MR), inter Landau level spacing are not enough to overcome Landau level broadening, and hence states are available in the vicinity of the Fermi level. This leads to finite resistance values in the low-field range. Also, in this low-field range, due to inter Landau level mixing, a positive MR effect is present [32], which offsets the negative MR and results in a weak overall MR. As the magnetic field is increased, inter Landau level spacing increases resulting in reduced inter Landau level mixing and around $B = B_{sw}$ the negative MR dominates the positive MR. We note that complete separation of the Landau levels is not necessary for observation of the negative MR. The negative MR should manifest whenever $n \rightarrow n$ tunneling dominates $n \rightarrow n'$ ($n \neq n'$) tunneling.

From the locations of the consecutive valleys in the MR oscillations in Figure 3(a), Landau level $n \sim 4$ (approximate value) is estimated to be occupied at field value $B \sim 5$ kG [44]. The inter Landau level spacing $E_5 - E_4$ and $E_4 - E_3$ is computed as 69.8 K and 79 K, respectively, and spacing between the lower order Landau levels is even higher. Clearly, MR oscillations are expected to occur at 50 K (assuming thermal broadening to be $\sim k_B T$, due to negligible defects as described before) and are expected to gradually disappear as temperature is increased beyond 80 K. At these higher temperatures, increased thermal broadening makes the Landau levels indistinguishable. The high field oscillations (Figure 3(a), 50 K data) have been shown in Figure SI-2(a) (Supplementary Information), after removing the nonoscillatory background. Sharp oscillations have been observed, which indicate formation of Landau levels. This is consistent with the quality of our samples, which did not show any measurable defect content in our Raman studies (Figures 1(a)–1(c)). It is important to note that the high field oscillations depend on the location of the Fermi level, which is dependent on (unintentional) doping of the samples.

Figure 3(b) displays the typical CPP MR of a thicker (~200 nm) MLG sample at three different temperatures. The zero-field resistance of this sample is 480 Ω at 50 K which gradually decreases to 190 Ω at 220 K. Clearly, this sample also shows insulating temperature dependence at zero field. Also noteworthy is the increase in zero-field resistance as compared to the thinner samples described above (both have nominally identical contact area). This implies that the CPP resistance originates from the graphene layers in the MLG "bulk" and not from the contacts or the interfaces. Unlike thinner MLG sample in Figure 3(a), the negative MR in this case is larger, ~92% at 50 K, and the negative MR clearly persists even at higher temperatures (~220 K). The inset in Figure 3(b) shows R_{zz}^{-1} versus B in the field range in which negative MR is most prominent. A clear linear fit has been observed, as expected from theory [31]. Further, slope of R_{zz}^{-1} versus B decreases with increasing temperature, which is also consistent with theory. This confirms that the observed effect originates from ILMR. As before, signs of high field oscillations have been observed in this sample for field values
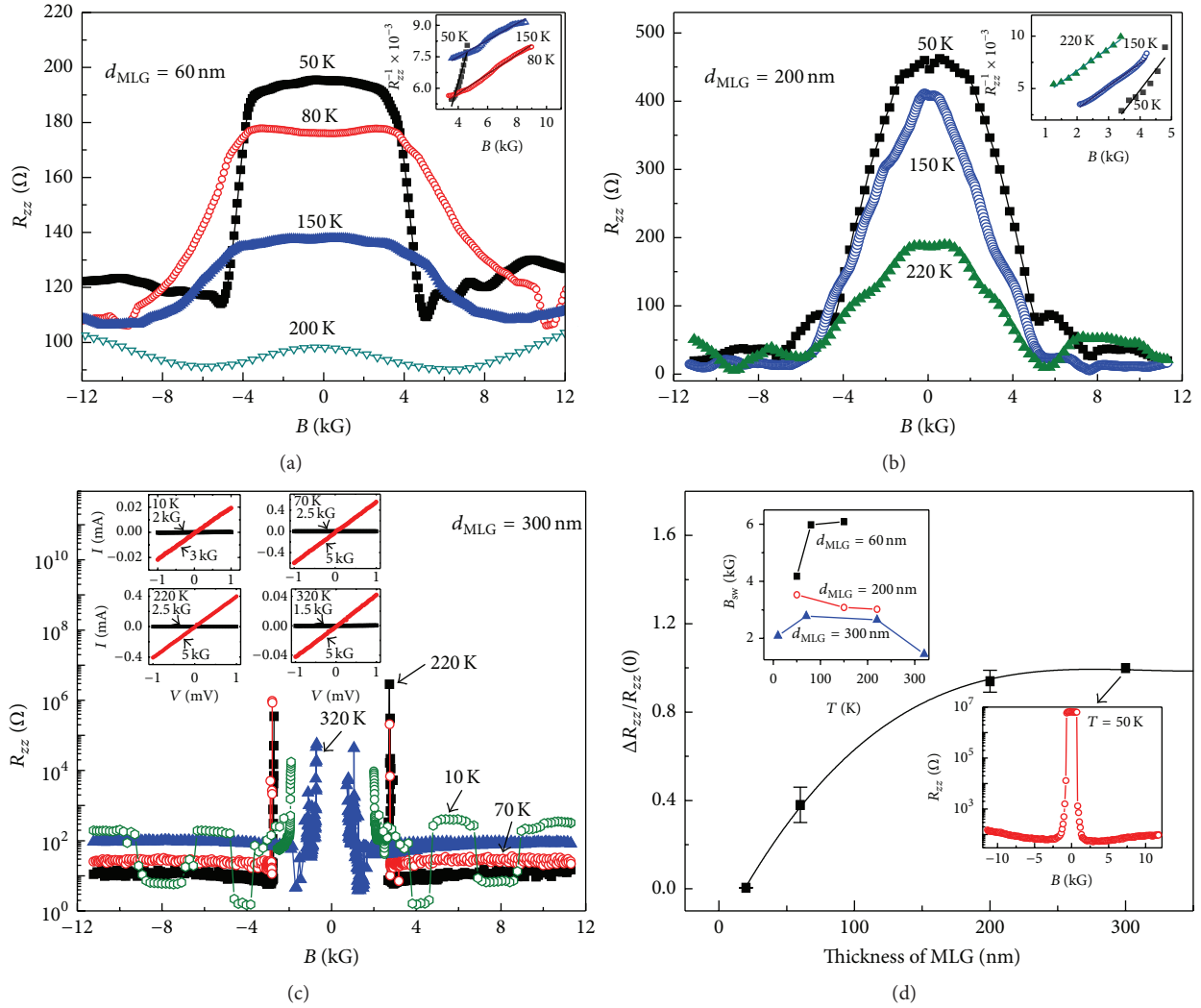
(a)

(b)

(c)

(d)

Figure 3: Interlayer magnetoresistance observed in weakly coupled MLG samples with various thicknesses. Data from (a) ~60 nm (batch S1), (b) ~200 nm (batch S2), and (c) ~300 nm (batch S3) samples are shown. At 50 K (Figure (a)), CPP resistance sharply drops with increasing magnetic field above B_{sw} ~ 4 kG and exhibits negative MR of ~40%. The negative MR effect becomes weaker as temperature is increased. For thicker MLG sample (Figure (b)), the negative MR is stronger, ~92% at 50 K. For samples with even larger thickness (Figure (c)), $R_{zz}(0)$ often exceeds the upper limit (100 MΩ) of the measurement apparatus, behaving as a virtual open circuit. However, as the perpendicular magnetic field is increased, resistance drops drastically by several orders of magnitude, resulting in a giant negative magnetoresistance that reaches theoretical maximum of ~100%. For all three sets of samples, average of both scan directions is presented at each temperature and no hysteresis has been observed. Each resistance value is the average of 50 readings. A constant DC current of 1 mA is applied to perform all MR measurements. The measured resistance values have been validated by using two different setups (Picotest multimeter and Keithley source meter). The insets in (a) and (b) show R_{zz}^{-1} versus B, and clear linear fits have been observed, which is consistent with the ILMR model. The top inset in Figure (c) shows magnetic field dependent switching of the I-V characteristics at various temperatures for the 300 nm sample. (d) MR ratio ($\Delta R_{zz}/R_{zz}(0) = |R_{zz}(B) - R_{zz}(0)|/R_{zz}(0)$) as a function of MLG thickness of as-grown MLG on Ni samples at 50 K. The magnetoresistance ratio increases with the thickness of MLG stack and almost reaches theoretical maximum (~100%) for thickness larger than 300 nm. Bottom inset shows data from a 300 nm thick sample which exhibits measurable finite $R_{zz}(0)$ of ~10^7 Ω. The MR data point corresponding to 300 nm thickness value in the main image is taken from this plot. The top inset shows B_{sw} versus T for the three batches. For 25 nm and 300 nm data points, error bars are smaller than marker size.

exceeding 4 kG. These oscillations have been plotted separately in Figure SI-2(b), after removing the nonoscillatory background (Supplementary Information). From the oscillations, we estimate Landau level n ~ 3 (approximate value) to be partially occupied at B ~ 5 kG. At 50 K and B ~ 5 kG, Landau levels n = 0–3 are completely separated and hence

such oscillations are expected. However, at ~150 K and higher, thermal broadening is larger than the inter Landau level spacing and oscillations are washed away.

As noted above, in Figures 3(a) and 3(b), MR effect is weak in the low-field regime (~0–3 kG range) and the sharp negative MR manifests outside this range. This is attributed

to a positive MR effect that is strong at the low-field range and offsets the negative MR mechanism. The positive MR can originate from two sources: (1) at low field, inter Landau level separation is smaller than Landau level broadening and significant inter Landau level mixing takes place. It has been shown in [32] that such inter Landau level mixing can produce positive MR effect in the low-field range. (2) Carriers undergo in-plane motion during interlayer transport. The in-plane component of charge transport exhibits positive MR [18]. Clearly these effects become stronger with increasing temperature and widens the negative MR (or increasing B_{sw}).

For the ~300 nm thick samples, some variations in the zero-field resistance have been observed. For example, in some samples $R_{zz}(0)$ is ~1.6 kΩ (Figure SI-1, Supplementary Information), as expected from the linear $R_{zz}(0)$ versus thickness plot in Figure 2(d). Typical CPP-MR response of such samples has been shown in Figure SI-1 (Supplementary information). This sample exhibits negative MR of ~88%. However, other ~300 nm thick samples show very high $R_{zz}(0)$, ~10^7 Ω or even higher (Figures 3(c) and 3(d) *bottom inset*, SI-1). In some cases, zero-field interlayer resistance exceeds the upper limit of our measurement system (100 MΩ). The negative MR effect in the $B \parallel I$ geometry is quite dramatic for these high resistance samples (Figure 3(c)). As shown in Figure 3(c), a relatively small perpendicular magnetic field of ~3 kG reduces the interlayer resistance by many orders of magnitude (note the logarithmic resistance scale in Figure 3(c)), leading to a giant MR with a switching ratio $(R_{zz}(0)/R_{zz}(B))$ of ~10^7. Discontinuity in the vicinity of the zero-field represents the range where the device resistance exceeds our instrumental limit. This effect persists at room temperature and has been recorded up to ~320 K (Figure 3(c)). To our knowledge, such strong negative MR has not been reported before in graphitic or any other system at comparable temperature and field range. At the lowest measurement temperature (10 K), strong MR oscillations have been observed, and Landau level $n \sim 2$ (approximate value) is estimated to be occupied. As before, these oscillations have been plotted separately in Figure SI-2(c) (Supplementary Information). Under these experimental conditions inter Landau level separation is larger than thermal broadening and hence oscillations are expected. The inset of Figure 3(c) shows the I-V characteristics of these thicker samples at two different field values, which clearly demonstrates a giant field dependent resistance switching. Figure 3(d), *bottom inset*, shows MR curve from a similar high resistance thick (~300 nm) specimen, which had a finite zero-field resistance of ~10^7 Ω. Figure SI-1 (Supplementary Information) shows data from two different ~300 nm samples, one with small zero-field resistance (~1.6 kΩ) and another which is virtually open circuit at zero field.

The large variation in the zero-field CPP resistance in the thick specimens most likely originates from the variation in the misorientation angle between the neighboring layers. The CPP resistance is not only determined by the number of graphene layers in the stack but it is also determined by the strength of interlayer coupling between the neighboring layers. Weak interlayer coupling will result in low probability of carrier transmission between the layers (at zero

magnetic field) and hence interlayer resistance is expected to be high. The very large zero-field resistance in the thick samples is presumably due to weaker interlayer coupling strength in thicker specimens. Interlayer coupling strength depends strongly on the extent of misorientation between the neighboring layers and small change in the misorientation angle can drastically affect interlayer resistance. Such effect has been investigated in [45, 46]. It has been found that a change in the misorientation angle from 0° to 30° can change interlayer resistance by 16 orders of magnitude. Clearly, this effect is not captured by the simple resistivity model in which R_{zz} is proportional to the MLG stack thickness. At present, we are unaware of any other reason that can explain such large variation in zero-field CPP resistance in nominally identical MLG specimens. In our studies we have found this effect only for the thick (~300 nm) samples and not for the other thinner samples. Clearly, the layers further away from the interface appear to become increasingly misoriented.

Figure 3(d) (*main image*) shows the MR as a function of the MLG stack thickness at 50 K. The MR ratio increases with the thickness of the MLG stack and almost reaches theoretical maximum (~100%, as mentioned before) for thickness ~300 nm or larger. As mentioned before, *bottom inset* of Figure 3(d) shows data from a ~300 nm thick sample which exhibited a finite measurable (high) resistance $R_{zz}(0) \sim 10^7$ Ω that corresponds to the 300 nm data point in the main plot.

A qualitative understanding of the thickness dependence of MR can be obtained as follows. MR ratio is primarily determined by the quantity $R_{zz}(0)/R_{zz}(B)$. The quantity $R_{zz}(0)$ depends strongly on the number of layers in the stack and also on the strength of the interlayer coupling as discussed above. Weaker interlayer coupling is expected to increase the value of $R_{zz}(0)$. As consistent with our experimental data presented above, thicker MLG stack results in larger $R_{zz}(0)$. On the other hand, the quantity $R_{zz}(B)$ depends on the number of carriers generated per unit volume in presence of a perpendicular magnetic field. Larger number of graphene layers in the MLG stack should result in an abundance of charge carriers and available states for interlayer tunneling and thereby smaller $R_{zz}(B)$ compared to the thinner layers. Combining these observations, stronger negative MR is expected in thicker MLGs.

Figure 3(d), *top inset*, shows B_{sw} as a function of temperature for all three thicknesses considered in this study. We observe that, for a given temperature, B_{sw} decreases with increasing thickness. This trend can be linked to the Landau level index n (at the Fermi level) that participates in the interlayer transport. As discussed above, in this study, n has been found to decrease with increasing thickness. Thus, for thicker samples smaller magnetic field will be needed to overcome Landau level mixing (and resulting positive MR) and trigger the negative MR. Lower n for thicker layers may result from the gradual decay in the charge density profile through the MLG stack from the doped (defective) interfacial layers.

We also note that, for 200 nm and 300 nm thick samples, B_{sw} tends to decrease with increasing temperature, especially in the higher temperature range (>150 K). We note that this feature is qualitatively different from what is expected in

the quantum limit, in which case $B_{\rm sw}$ increases quadratically with temperature [31]. A possible reason for this anomaly could be the temperature dependence of the Fermi level, which is known to move at lower energy values as temperature is increased [47]. The critical parameter is the Fermi temperature $T_F = E_F/k_B$, and Fermi level decreases drastically (by a factor of ~2) in the range $T/T_F \sim 0.35$–0.9 [47]. As the Fermi level decreases with increasing temperature, lower order Landau levels will participate in the interlayer charge transport at higher temperatures. For lower order Landau levels, smaller B will be needed to reduce the effect of inter Landau level mixing and trigger the negative MR. This will lead to a reduction in $B_{\rm sw}$ (for a given sample) as temperature is increased.

Lowering of the Fermi level with temperature is more pronounced at higher temperature [47], and this is presumably the reason why the reduction of $B_{\rm sw}$ with T is not significant in the low T regime and has not been observed at all for the 60 nm sample, in which case negative MR disappears at a much lower temperature. For example, in the case of 300 nm samples, from the oscillations at 10 K we had estimated Landau level ~2 (approximate value) to be occupied at 4 kG (see previous discussions). This translates to $E_F \sim 32.4$ meV and $T_F \sim 374$ K. Thus, over the measurement range of 10 K–320 K, T/T_F varies from 0.026 to 0.85, thus implying a large change (by factor of ~2) in the location of the Fermi level over the temperature range of 10–320 K and a resulting significant decrease in $B_{\rm sw}$. We note that, at 320 K, thermal broadening (estimated as $k_B T$) is ~27 meV and the above-mentioned twofold drop in the Fermi level will push it below the thermally broadened range (320 K) of its low-temperature value (32.4 meV). After this twofold drop, the Fermi level will be located ~16.2 meV, and this energy range is primarily dominated by (thermally broadened) Landau levels 0 and 1 in the field range considered. Clearly, lower Landau levels are participating in transport at higher temperatures and smaller $B_{\rm sw}$ is expected.

Performing similar estimates for the other two batches, we find that T/T_F varies in the (narrower) range 0.09–0.43 for 200 nm samples and 0.08–0.33 for 60 nm samples. Thus, change in the Fermi level is less drastic in these batches (by a factor of ~1.2–1.4). Further, as discussed above, in these samples Fermi levels are located at higher energy values at low temperatures. Thus, resulting reduction in $B_{\rm sw}$ is relatively less compared to the 300 nm batch. We note that no theoretical model exists at this point that addresses such scenarios and further theoretical studies are required to obtain a quantitative understanding of this effect.

In conclusion, in this work we demonstrated ILMR effect in MLG stacks of various thicknesses. It has been found that the ILMR effect persists and becomes stronger as thickness is increased. Also, for larger thickness samples, magnitude of the MR effect is relatively insensitive to temperature. This is consistent with our prior work in [16]. This is in significant contrast with spintronic based MR devices such as GMR or spin valves. In spintronic devices, thickness of the "active" spin transport layer needs to be smaller than typical "spin relaxation length" of the material that constitutes the active region [48]. This imposes significant limitation on the device

geometry and requires stringent control over the fabrication steps. Larger thickness of the "active" layer generally reduces the MR signal and smaller thickness leads to reliability issues such as formation of pinhole shorts between the electrodes. Also, for spintronic devices signal strength tends to decrease with increasing temperature. Due to these factors, ILMR effect in MLG appears to be a more robust MR mechanism for practical applications. Further, intrinsic compatibility of MLG with flexible electronics and sensorics makes ILMR an exciting platform for future magnetic sensing and data storage technologies.

Disclosure

Competing Interests

The authors declare that they have no competing interests.

Acknowledgments

References

[1] K. S. Novoselov, Z. Jiang, Y. Zhang et al., "Room-temperature quantum hall effect in graphene," *Science*, vol. 315, no. 5817, p. 1379, 2007.

[2] A. K. Geim and K. S. Novoselov, "The rise of graphene," *Nature Materials*, vol. 6, no. 3, pp. 183–191, 2007.

[3] K. S. Novoselov, A. K. Geim, S. V. Morozov et al., "Two-dimensional gas of massless Dirac fermions in graphene," *Nature*, vol. 438, no. 7065, pp. 197–200, 2005.

[4] S. Das Sarma, S. Adam, E. H. Hwang, and E. Rossi, "Electronic transport in two-dimensional graphene," *Reviews of Modern Physics*, vol. 83, no. 2, pp. 407–470, 2011.

[5] G. Li and E. Y. Andrei, "Observation of Landau levels of Dirac fermions in graphite," *Nature Physics*, vol. 3, no. 9, pp. 623–627, 2007.

[6] Y. Kopelevich, J. H. S. Torres, R. R. da Silva, L. F. Mrowka, H. Kempa, and P. Esquinzi, "Reentrant metallic behavior of graphite in the quantum limit," *Physical Review Letters*, vol. 90, no. 15, Article ID 156402, 2003.

[7] H. Kempa, P. Esquinazi, and Y. Kopelevich, "Integer quantum Hall effect in graphite," *Solid State Communications*, vol. 138, no. 3, pp. 118–122, 2006.

[8] C. Berger, Z. Song, T. Li et al., "Ultrathin epitaxial graphite: 2D electron gas properties and a route toward graphene-based nanoelectronics," *Journal of Physical Chemistry B*, vol. 108, no. 52, pp. 19912–19916, 2004.

[9] Y. Kopelevich and P. Esquinazi, "Graphene physics in graphite," *Advanced Materials*, vol. 19, no. 24, pp. 4559–4563, 2007.

[10] K. S. Novoselov, V. I. Fal'Ko, L. Colombo, P. R. Gellert, M. G. Schwab, and K. Kim, "A roadmap for graphene," *Nature*, vol. 490, no. 7419, pp. 192–200, 2012.

[11] Y. Zhang, L. Zhang, and C. Zhou, "Review of chemical vapor deposition of graphene and related applications," *Accounts of Chemical Research*, vol. 46, no. 10, pp. 2329–2339, 2013.

[12] A. N. Pal and A. Ghosh, "Ultralow noise field-effect transistor from multilayer graphene," *Applied Physics Letters*, vol. 95, no. 8, Article ID 082105, 2009.

[13] J.-J. Chen, J. Meng, Y.-B. Zhou et al., "Layer-by-layer assembly of vertically conducting graphene devices," *Nature Communications*, vol. 4, article 1921, 2013.

[14] V. M. Karpan, G. Giovannetti, P. A. Khomyakov et al., "Graphite and graphene as perfect spin filters," *Physical Review Letters*, vol. 99, no. 17, Article ID 176602, 2007.

[15] T. Banerjee, W. G. Van Der Wiel, and R. Jansen, "Spin injection and perpendicular spin transport in graphite nanostructures," *Physical Review B—Condensed Matter and Materials Physics*, vol. 81, no. 21, Article ID 214409, 2010.

[16] S. C. Bodepudi, A. P. Singh, and S. Pramanik, "Giant current-perpendicular-to-plane magnetoresistance in multilayer graphene as grown on nickel," *Nano Letters*, vol. 14, no. 5, pp. 2233–2241, 2014.

[17] S. C. Bodepudi, X. Wang, and S. Pramanik, "Angle dependent interlayer magnetoresistance in multilayer graphene stacks," *Journal of Applied Physics*, vol. 118, no. 16, Article ID 164303, 2015.

[18] Z.-M. Liao, H.-C. Wu, S. Kumar et al., "Large magnetoresistance in few layer graphene stacks with current perpendicular to plane geometry," *Advanced Materials*, vol. 24, no. 14, pp. 1862–1866, 2012.

[19] A. L. Friedman, J. L. Tedesco, P. M. Campbell et al., "Quantum linear magnetoresistance in multilayer epitaxial graphene," *Nano Letters*, vol. 10, no. 10, pp. 3962–3965, 2010.

[20] H. Kempa, P. Esquinazi, and Y. Kopelevich, "Field-induced metal-insulator transition in the c-axis resistivity of graphite," *Physical Review B—Condensed Matter and Materials Physics*, vol. 65, no. 24, Article ID 241101, 2002.

[21] J. E. Lenz, "A review of magnetic sensors," *Proceedings of the IEEE*, vol. 78, no. 6, pp. 973–989, 1990.

[22] G. A. Prinz, "Magnetoelectronics," *Science*, vol. 282, no. 5394, pp. 1660–1663, 1998.

[23] B. Partoens and F. M. Peeters, "From graphene to graphite: electronic structure around the K point," *Physical Review B—Condensed Matter and Materials Physics*, vol. 74, no. 7, Article ID 075404, 2006.

[24] H. Min and A. H. MacDonald, "Electronic structure of multilayer graphene," *Progress of Theoretical Physics Supplement*, no. 176, pp. 227–252, 2008.

[25] S. Shallcross, S. Sharma, E. Kandelaki, and O. A. Pankratov, "Electronic structure of turbostratic graphene," *Physical Review B*, vol. 81, no. 16, Article ID 165105, 15 pages, 2010.

[26] L. M. Malard, M. A. Pimenta, G. Dresselhaus, and M. S. Dresselhaus, "Raman spectroscopy in graphene," *Physics Reports*, vol. 473, no. 5-6, pp. 51–87, 2009.

[27] A. Reina, X. Jia, J. Ho et al., "Large area, few-layer graphene films on arbitrary substrates by chemical vapor deposition," *Nano Letters*, vol. 9, no. 1, pp. 30–35, 2009.

[28] A. Luican, G. Li, A. Reina et al., "Single-layer behavior and its breakdown in twisted graphene layers," *Physical Review Letters*, vol. 106, no. 12, Article ID 126802, 2011.

[29] N. Tajima, S. Sugawara, R. Kato, Y. Nishio, and K. Kajita, "Effect of the zero-mode Landau level on interlayer magnetoresistance in multilayer massless dirac fermion systems," *Physical Review Letters*, vol. 102, no. 17, Article ID 176403, 2009.

[30] N. Tajima, M. Sato, S. Sugawara, R. Kato, Y. Nishio, and K. Kajita, "Spin and valley splittings in multilayered massless Dirac fermion system," *Physical Review B*, vol. 82, no. 12, Article ID 121420, 2010.

[31] T. Osada, "Negative interlayer magnetoresistance and zero-mode Landau level in multilayer Dirac electron systems," *Journal of the Physical Society of Japan*, vol. 77, no. 8, Article ID 084711, 2008.

[32] T. Morinari and T. Tohyama, "Crossover from positive to negative interlayer magnetoresistance in multilayer massless dirac fermion system with non-vertical interlayer tunneling," *Journal of the Physical Society of Japan*, vol. 79, no. 4, Article ID 044708, 2010.

[33] S. C. Bodepudi, A. P. Singh, and S. Pramanik, "Current-perpendicular-to-plane magnetoresistance in chemical vapor deposition-grown multilayer graphene," *Electronics*, vol. 2, no. 3, pp. 315–331, 2013.

[34] Z. Ni, Y. Wang, T. Yu, and Z. Shen, "Raman spectroscopy and imaging of graphene," *Nano Research*, vol. 1, no. 4, pp. 273–291, 2008.

[35] J. Wintterlin and M.-L. Bocquet, "Graphene on metal surfaces," *Surface Science*, vol. 603, no. 10–12, pp. 1841–1852, 2009.

[36] K. Kanzaki, H. Hibino, and T. Makimoto, "Graphene layer formation on polycrystalline nickel grown by chemical vapor deposition," *Japanese Journal of Applied Physics*, vol. 52, no. 3, Article ID 035103, 2013.

[37] L. Baraton, Z. B. He, C. S. Lee et al., "On the mechanisms of precipitation of graphene on nickel thin films," *EPL Europhysics letters*, vol. 96, no. 4, Article ID 46003, 2011.

[38] Q. Yu, J. Lian, S. Siriponglert, H. Li, Y. P. Chen, and S.-S. Pei, "Graphene segregated on Ni surfaces and transferred to insulators," *Applied Physics Letters*, vol. 93, no. 11, Article ID 113103, 2008.

[39] F. Fiorillo, "Basic phenomenology in magnetic materials," in *Measurement and Characterization of Magnetic Materials*, pp. 3–24, Elsevier Academic Press, Amsterdam, The Netherlands, 1st edition, 2004.

[40] F. Fiorillo, C. Appino, and M. Pasquale, "Hysteresis in magnetic materials," in *The Science of Hysteresis*, vol. 3, Elsevier Academic Press, New York, NY, USA, 2006.

[41] D. E. Soule, J. W. McClure, and L. B. Smith, "Study of the Shubnikov-de Haas effect. Determination of the fermi surfaces in graphite," *Physical Review*, vol. 134, no. 2, pp. A453–A470, 1964.

[42] R. F. Pires, P. Pureur, M. Behar, J. L. Pimentel Jr., J. Schaf, and Y. Kopelevich, "Magnetism, magnetoresistance, and Shubnikov-de Haas oscillations in Na-implanted highly oriented pyrolitic graphite," *Journal of Applied Physics*, vol. 111, no. 9, Article ID 093922, 2012.

[43] X. C. Yang, H. M. Wang, T. R. Wu et al., "Magnetotransport of polycrystalline graphene: shubnikov-de Haas oscillation and weak localization study," *Applied Physics Letters*, vol. 102, no. 23, Article ID 233503, 2013.

[44] S. Datta, *Electronic Transport in Mesoscopic Systems*, Cambridge University Press, Cambridge, UK, 1995.

[45] R. Bistritzer and A. H. MacDonald, "Transport between twisted graphene layers," *Physical Review B—Condensed Matter and Materials Physics*, vol. 81, no. 24, Article ID 245412, 2010.

[46] K. M. M. Habib, S. S. Sylvia, S. Ge, M. Neupane, and R. K. Lake, "The coherent interlayer resistance of a single, rotated interface between two stacks of AB graphite," *Applied Physics Letters*, vol. 103, no. 24, Article ID 243114, 2013.

[47] E. H. Hwang and S. Das Sarma, "Screening-induced temperature-dependent transport in two-dimensional graphene," *Physical Review B*, vol. 79, no. 16, Article ID 165404, 2009.

[48] C. Chappert, A. Fert, and F. N. Van Dau, "The emergence of spin electronics in data storage," *Nature Materials*, vol. 6, no. 11, pp. 813–823, 2007.

Journal of
Nanotechnology

International Journal of
Corrosion

International Journal of
Polymer Science

Smart Materials
Research

Journal of
Composites

BioMed
Research International

Journal of
Metallurgy

Journal of
Materials
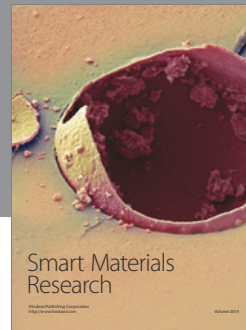
Hindawi

Submit your manuscripts at
http://www.hindawi.com

Journal of
Nanoparticles

Advances in
Materials Science and Engineering

Scientifica

Journal of
Nanomaterials

The Scientific
World Journal

International Journal of
Biomaterials

Journal of
Nanoscience

Journal of
Coatings

Journal of
Crystallography

Journal of
Ceramics

Journal of
Textiles